Supplement of Atmos. Chem. Phys., 26, 16295–16308, 2026
https://doi.org/10.5194/acp-26-16295-2026-supplement
© Author(s) 2026. CC BY 4.0 License.



Atmospheric Chemistry and Physics
Open Access
EGU

Supplement of

Temperature-dependent evaporation emission and gas/particle partitioning drive the seasonal dynamics of primary intermediate-volatility organic compounds

Hua Fang et al.

Correspondence to: Ting Wu (wuting19@mail.ahnu.edu.cn) and Xinming Wang (wangxm@gig.ac.cn)

The copyright of individual parts of the supplement might differ from the article licence.

S1. Online GC-MSD/FID analysis

VOC species were measured using an online gas chromatography system equipped with both a mass spectrometric detector (MSD) and a flame ionization detector (FID). A Teflon filter was installed upstream of the sampling inlet to remove particles from the air stream. Ambient air was collected and concentrated using an electronically refrigerated pre-concentrator. The system operated through two parallel channels: one channel, equipped with a PLOT column (25 m × 0.32 mm × 8 μm, Agilent Technologies) and the FID, was dedicated to analyzing lower-molecular-weight non-methane hydrocarbons; the other channel, equipped with a DB-624 column (60 m × 0.25 mm × 1.4 μm, J&W Scientific) and the MSD, analyzed the remaining VOCs. In the FID channel, ambient air was trapped at −20 °C to remove most of the water vapor, and CO_2 was subsequently removed using a CO_2 adsorption tube. In the MSD channel, air was similarly trapped and dewatered at −20 °C. The VOCs from both channels were then transferred by helium and focused at −160 °C. Following this, the trap was rapidly heated to 120 °C to desorb the target compounds into the GC column. The GC oven temperature was programmed as follows: initial hold at 35 °C for 3 min, increased to 150 °C at 5 °C min^{-1}, then further raised to 190 °C at 10 °C min^{-1}, and finally held at 190 °C for 8 min. The MSD was operated in selected ion monitoring (SIM) mode with electron impact ionization at 70 eV.

S2. PMF model running process

To determine the optimal number of factors, PMF model (USEPA PMF 5.0) was run with factor numbers ranging from 3 to 8. The stability of each solution was evaluated through bootstrap analysis (100 runs, R = 0.6). A stable model is indicated by the successful mapping of base run factors in 100 bootstrap runs. Moreover, the model output with a mapping rate above 80% suggests interpretable bootstrap uncertainties and an appropriate factor number. As shown in Table S1, we identified the solutions with three and four factors as the most stable. In lights of highly agreement between predicted and observed results (Figure S13), a four-factor resolution was finally selected. The values of Q_{robust} and Q_{true} were equal for all the 100 runs. The calculated R^2 values of all species that input into the model were all greater than 0.69. Furthermore, we also applied K-means clustering to explore the predominant category of measured IVOCs. The mathematical details of K-means clustering are described elsewhere (Hartigan and Wong, 1979), and the relevant code is available at https://github.com/JayshKhan/KmeanVisualizing. Based on the elbow method, the optimal number of clusters was determined to be four (Figure S14), further supporting the four-factor resolution identified by the PMF model.

Due to the absence of low-volatility IVOCs (e.g., nC_{18}–nC_{20}) in winter samples, a separate PMF analysis was performed for this season using 14 species as input (Figure S15). Factor identification, determination of factor number, and model evaluation followed the same procedures applied in other seasons. As shown in Figure S15, factor 1 was attributed to vehicle exhaust, characterized by high loadings of Nap, CO, NO_2 and nC_{12}-nC_{14}. Factor 2, with high moderate-volatility IVOCs but low CO and NO_2, was identified as evaporative emissions. Factor 3, distinguished by abundant low-volatility IVOCs alongside extremely high CO and NO_2, was associated with gas/particle partitioning. Factor 4, rich in SO_2, CO, and NO_2, was interpreted as industrial emission. The model reliably reproduced observed winter IVOC concentrations (slope = 0.95, R^2 = 0.98).

Table S1. The result of bootstrap (BS) simulation with different number of factors.

BS Mapping (Factors=3)

	Base Factor 1	Base Factor 2	Base Factor 3	Unmapped
Boot Factor 1	100	0	0	0
Boot Factor 2	0	100	0	0
Boot Factor 3	0	0	100	0

BS Mapping (Factors=4)

	Base Factor 1	Base Factor 2	Base Factor 3	Base Factor 4	Unmapped
Boot Factor 1	100	0	0	0	0
Boot Factor 2	0	100	0	0	0
Boot Factor 3	0	0	100	0	0
Boot Factor 4	0	0	0	100	0

BS Mapping (Factors=5)

	Base Factor 1	Base Factor 2	Base Factor 3	Base Factor 4	Base Factor 5	Unmapped
Boot Factor 1	99	0	1	0	0	0
Boot Factor 2	0	100	0	0	0	0
Boot Factor 3	0	0	100	0	0	0
Boot Factor 4	0	0	6	93	0	1
Boot Factor 5	0	0	0	1	99	0

BS Mapping (Factors=6)

	Base Factor 1	Base Factor 2	Base Factor 3	Base Factor 4	Base Factor 5	Base Factor 6	Unmapped
Boot Factor 1	95	0	0	0	4	1	0
Boot Factor 2	0	100	0	0	0	0	0
Boot Factor 3	0	0	100	0	0	0	0
Boot Factor 4	0	0	0	100	0	0	0
Boot Factor 5	1	0	13	0	82	3	1

Boot Factor 6	2	1	5	0	2	90	0	

BS Mapping (Factors=7)

	Base Factor 1	Base Factor 2	Base Factor 3	Base Factor 4	Base Factor 5	Base Factor 6	Base Factor 7	Unmapped
Boot Factor 1	98	2	0	0	0	0	0	0
Boot Factor 2	0	92	1	2	1	0	2	2
Boot Factor 3	0	0	99	0	0	0	1	0
Boot Factor 4	0	0	0	100	0	0	0	0
Boot Factor 5	0	0	0	0	100	0	0	0
Boot Factor 6	0	1	0	0	0	97	2	0
Boot Factor 7	0	1	0	0	0	0	99	0

BS Mapping (Factors=8)

	Base Factor 1	Base Factor 2	Base Factor 3	Base Factor 4	Base Factor 5	Base Factor 6	Base Factor 7	Base Factor 8	Unmapped
Boot Factor 1	93	0	0	0	1	1	0	5	0
Boot Factor 2	0	99	0	0	1	0	0	0	0
Boot Factor 3	0	0	100	0	0	0	0	0	0
Boot Factor 4	0	0	0	100	0	0	0	0	0
Boot Factor 5	0	1	0	0	99	0	1	0	0
Boot Factor 6	0	0	0	0	0	100	0	0	0
Boot Factor 7	1	0	0	0	0	3	96	0	0
Boot Factor 8	1	0	18	0	1	10	0	70	0

Table S2. $PM_{2.5}$, gas pollutants and meteorological parameters recorded in four seasons.

	Spring (March, April, May)			Summer (June, July, August)			Fall (September, October, November)			Winter (December, January, February)		
	Ave±95%C.I.	Min-Max	Median	Ave±95%C.I.	Min-Max	Median	Ave±95%C.I.	Min-Max	Median	Ave±95%C.I.	Min-Max	Median
SO_2 (μg/m^3)	8.1±0.1	5.0−22.0	8	7.7±0.1	5.0−15.0	8	8.7±0.1	5.0−21.0	8	9.7±0.2	4.0-27.0	10
NO_2 (μg/m^3)	32.1±0.7	8.0−120.0	28	17.8±0.4	3.0−104.0	16	28.2±0.6	6.0−98.0	24	40.4±1.1	4.0-126.0	37
CO (mg/m^3)	0.7±0.0	0.3−1.6	0.6	0.6±0.0	0.3−1.6	0.6	0.7±0.0	0.2−1.7	0.6	0.8±0.0	0.3-2.2	0.7
O_3 (μg/m^3)	65.4±1.5	2.0−190.0	60	103.8±1.9	5.0−252.0	97	84.4±1.9	2.0−214.0	77	46.9±1.3	2.0-145.0	45
PM_{10} (μg/m^3)	60.6±1.4	3.0−225.0	53	30.1±0.6	3.0−93.0	29	42.4±0.8	3.0−149.0	40	93.2±1.9	19.0-356.0	87
$PM_{2.5}$ (μg/m^3)	32.4±0.7	2.0−95.0	30	16.6±0.4	2.0−48.0	15	22.6±0.5	2.0−84.0	20	60.2±1.6	8.0-272.0	56
Temperature (°C)	17.8±0.3	-1.2−33.1	18	29.3±0.2	18.1−39.3	29.3	20.0±0.3	4.6−37.3	19.3	5.7±0.2	-6.2-21.4	6
Relative humidity (%)	74.8±0.8	24.0−99.0	78	72.3±0.7	30.0−98.0	73	76.5±0.7	18.0−99.0	79	63.4±1.0	14.0-99.0	64
Wind speed (m/s)	2.0±0.0	0.0−6.5	1.9	2.2±0.0	0.0−9.4	2	2.7±0.1	0.0−10.7	2.5	2.2±0.1	0.1-10.6	1.7
Wind direction (°)	131.4±3.8	1.0−360.0	101	156.6±3.2	0.0−360.0	144	128.2±4.7	0.0−357.0	87	161.7±4.8	0.0-358.0	135
Atmospheric pressure (hPa)	1012.5±0.3	998.0−1031.0	1011	1002.1±0.2	993.0−1014.0	1001	1017.0±0.3	1002.0−1032.0	1018	1025.7±0.2	1011.0-1040.0	1026

Table S3. Averages of meausred IVOC species (ng m^{-3}), $PM_{2.5}$, gas pollutants and meteorological parameters during the observed periods.

Species	**Spring** (April 21−27)		**Summer** (July 4−10)		**Fall** (October 9−15)		**Winter** (December 14−20)		**Entire observed period**	
	Ave	**95%C.I.**	**Ave**	**95%C.I.**	**Ave**	**95%C.I.**	**Ave**	**95%C.I.**	**Ave**	**95%C.I.**
Naphthalene	112.9	20.1	77.7	7.9	108.4	18.8	116.7	24.6	104.2	9.7
1-Methylnaphthalene	21.2	4.4	31.7	6.7	25.7	5.0	19.3	3.5	24.3	2.6
2-Methylnaphthalene	11.7	2.3	14.9	3.0	14.3	2.9	10.3	1.9	12.7	1.3
Dodecane	130.6	26.8	63.8	10.6	128.1	26.3	80.5	13.1	100.6	10.9
Tridecane	108.8	16.1	129.3	21.1	97.8	13.3	103.5	28.4	109.9	10.5
Tetradecane	222.6	57.2	378.7	103.9	120.2	17.5	58.8	8.4	194.3	33.8
Pentadecane	179.7	24.8	333.1	70.0	149.9	21.5	61.9	8.4	179.8	23.1
Hexadecane	139.9	23.2	379.7	100.8	175.9	38.5	38.8	6.8	181.0	31.6
Heptadecane	79.9	7.9	129.7	28.4	113.6	20.1	22.9	4.3	85.3	10.3
Octadecane	28.2	2.4	189.2	55.2	39.2	6.6	6.1	0.8	81.7	18.3
Nonadecane	14.2	1.3	28.6	2.2	12.3	1.0	ND	ND	18.2	1.3
Eicosane	18.0	2.8	62.1	12.4	10.7	0.9	11.9	2.9	26.8	4.4
Heneicosane	39.0	4.5	64.8	8.4	12.2	1.6	1.4	0.2	29.3	4.1
Docosane	39.3	3.6	98.7	8.9	18.5	1.9	1.4	0.3	40.4	5.5
Pristane	31.6	5.0	52.4	13.8	114.3	25.4	5.5	1.6	55.6	8.9
Phytane	14.9	2.4	38.4	7.6	17.8	2.9	ND	ND	23.6	2.8
C_{12}-C_{13}	239.3	41.6	193.1	23.8	221.5	39.0	184.0	33.2	210.5	17.7
C_{14}-C_{15}	402.3	78.4	711.8	167.3	265.0	38.5	120.7	15.9	374.0	54.9
C_{16}-C_{17}	219.7	29.7	509.4	126.5	283.9	58.5	61.7	10.9	266.3	40.8
C_{18}-C_{19}	42.4	3.4	217.8	56.7	50.5	7.6	6.2	2.3	76.8	17.8
C_{20}-C_{22}	96.3	9.7	225.6	20.6	40.6	4.3	10.4	3.1	92.8	12.4

PAHs	145.8	24.5	124.4	16.6	148.4	25.7	146.3	29.3	141.3	12.3
Long-chain alkanes	1046.5	140.7	1948.5	371.5	1010.4	148.0	381.8	43.7	1087.0	128.1
ΣIVOCs	1192.2	153.5	2072.9	384.3	1158.8	168.8	528.1	65.4	1228.2	132.7
CPI	0.91	0.07	0.81	0.07	0.87	0.04	1.26	0.25	0.86	0.03
SO_2 (μg/m^3)	6.6	0.3	6.4	0.3	9.1	0.3	14.3	1.0	9.1	0.5
CO (mg/m^3)	0.5	0.0	0.6	0.1	0.8	0.1	0.8	0.1	0.7	0.0
O_3 (μg/m^3)	71.8	7.1	122.6	13.1	95.4	11.0	42.4	6.4	82.9	6.3
$PM_{2.5}$ (μg/m^3)	27.9	2.3	12.6	1.4	31.0	2.5	50.6	5.2	30.8	2.4
NO_2 (μg/m^3)	24.9	2.9	16.5	4.1	26.1	2.7	41.1	4.8	27.3	2.2
Temperature (°C)	21.6	0.7	33.1	0.8	20.9	0.8	4.9	1.0	19.9	1.4
Relative humidity (%)	63.1	3.8	63.6	3.2	74.2	5.1	58.5	5.6	64.6	2.4
Wind speed (m/s)	2.4	0.3	2.2	0.2	2.1	0.3	2.3	0.4	2.3	0.2
Wind direction (°)	55.2	13.1	182.0	12.3	118.6	15.3	208.2	23.0	140.9	11.5
Atmospheric pressure (hPa)	1005.4	0.7	1000.4	0.4	1016.7	0.4	1028.5	1.1	1012.8	1.5
Atmospheric boundary layer height (m)	549.8	100.3	819.2	126.4	500.8	98.6	496.0	118.1	590.4	58.2

Table S4. Concentrations of ambient long-chain normal alkanes in particle and gas phase reported in previous studies and this study.

Phase	Studied area	Sampling period	Range	Concentration (ng m^{-3})	References
Particle	Beijing	2020.11-2021.10	nC_{13}−nC_{40}	4.51−153 (32.7)*	Yang et al., 2023
	Shanghai	2013	nC_{8}−nC_{40}	228	Lyu et al., 2016
	Guangzhou	2012 winter	nC_{14}−nC_{40}	103±74	Wang et al., 2016
		2012 Summer	nC_{14}−nC_{40}	26±7	
	Nanjing	2014.11-2015.08	nC_{16}−nC_{40}	83.8±57.1	Hong et al., 2017
	Seoul	2018.01-2018.02	nC_{20}−C_{36}	28.4±16.4	Kang et al., 2020
		2018.03-2018.04		16.4±12.5	
		2018.08-2018.09		6.4±2.5	
		2018.11-2018.12		16.3±7.1	
Gas	London	2017.01-2017.04	nC_{13}−nC_{36}	32.4−141.0	Xu et al.,
	Beijing	2018.02-2018.07	nC_{12}−nC_{21}	1168±361	Tang et al., 2022
	Guangzhou	2019.09-2019.10	nC_{12}−nC_{22}	1296.1±673.5	Fang et al., 2022
	Wuhu	2024.04	nC_{12}−nC_{22}	1000.0±135.1	This study
		2024.07		1857.7±283.5	
		2024.10		878.3±120.3	
		2024.12		377.6±42.9	

* average

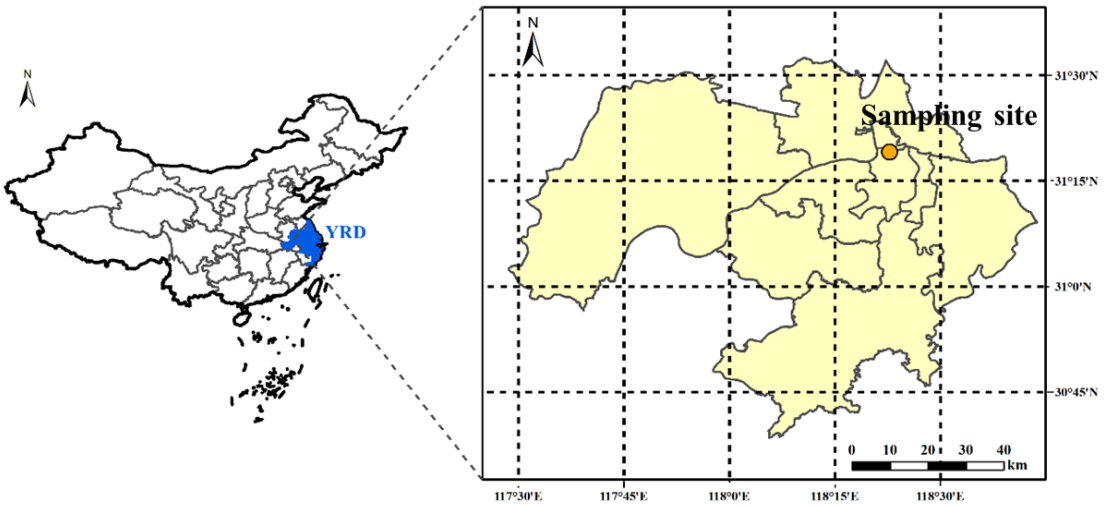


Figure S1. The geographical location of observation site. The map was created by the authors using MeteoInfo (http://www.meteothink.org), an open-source software developed by Wang et al. (2014).

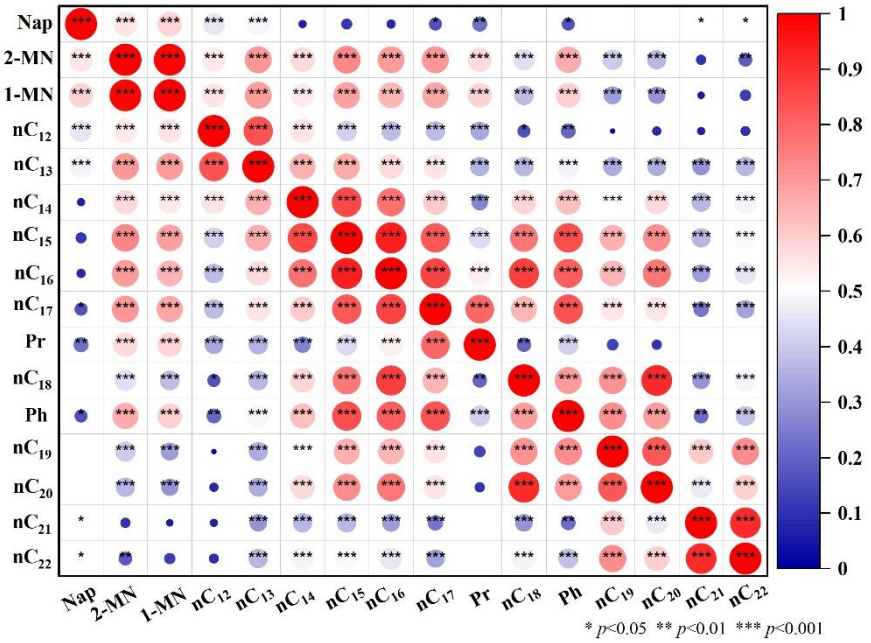


Figure S2. Correlation matrix of sixteen IVOC species measured during the sampling periods.

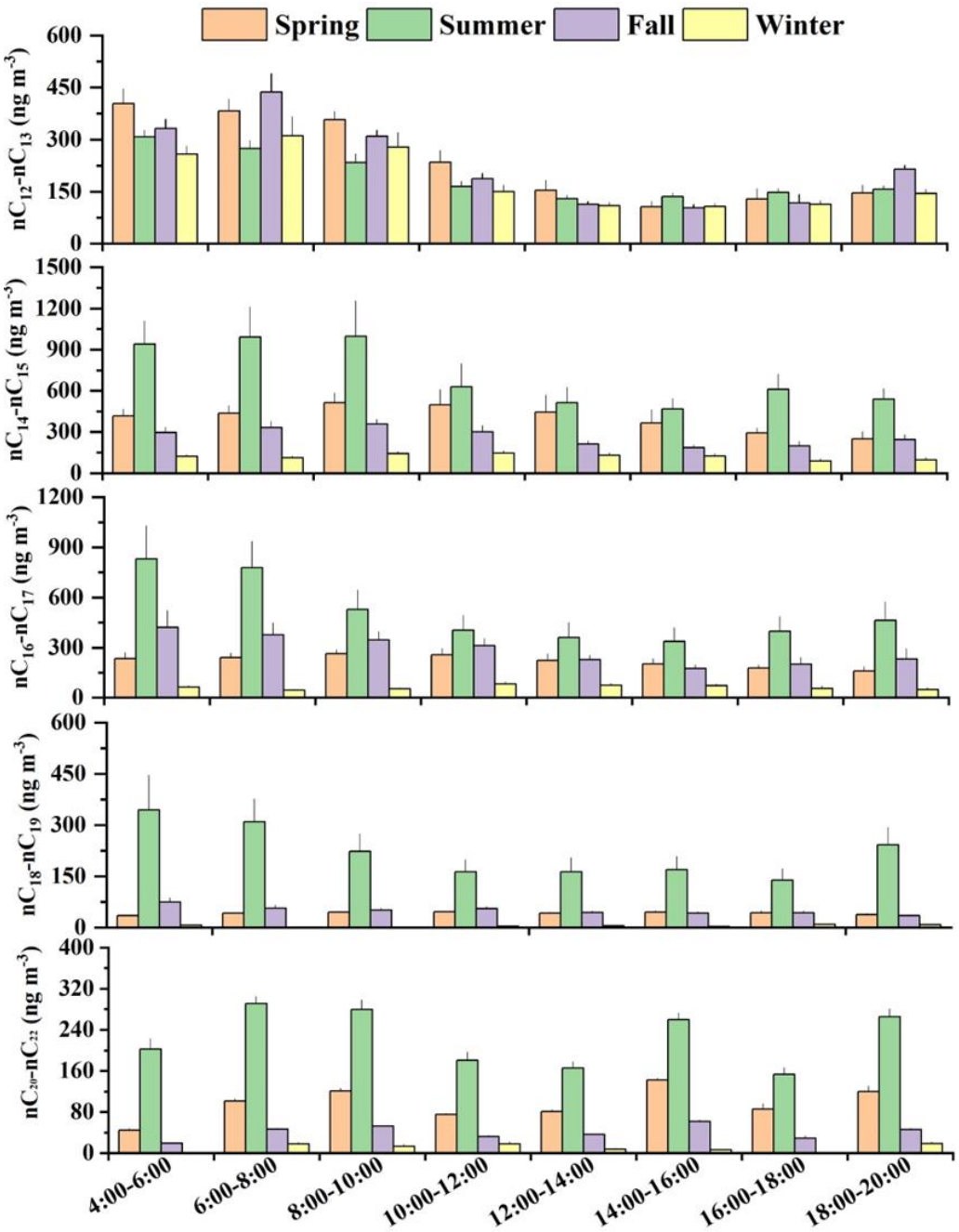


Figure S3. Diurnal variations of measured IVOCs in four seasons. Error bar is 95% confidence interval.

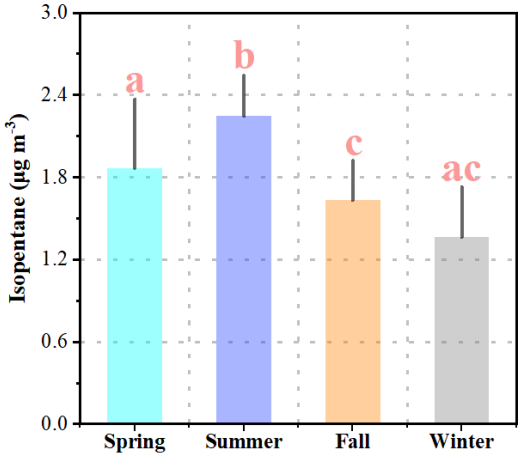


Figure S4. Seasonal difference of isopentane measured in this study. Error bar is 95% confidence intervals. Different letters denote statistically significant differences at $p < 0.05$.

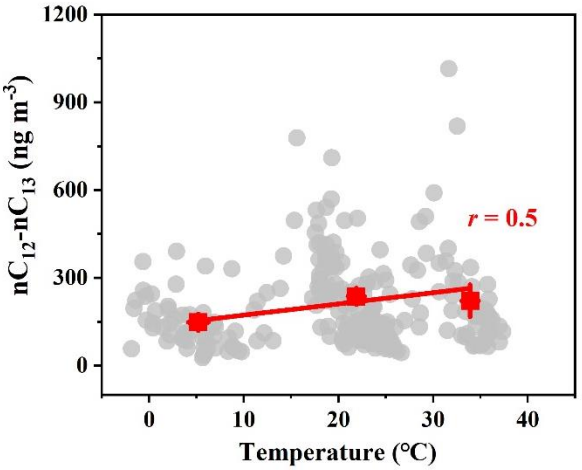


Figure S5. Relationship between C_{12}-C_{13} concentration and temperature observed during the sampling. Gray scatters were the original data, and red pane was the average in three temperature intervals: < 15°C, 15−30°C and >30°C. Error bar represents 95% confidence interval.

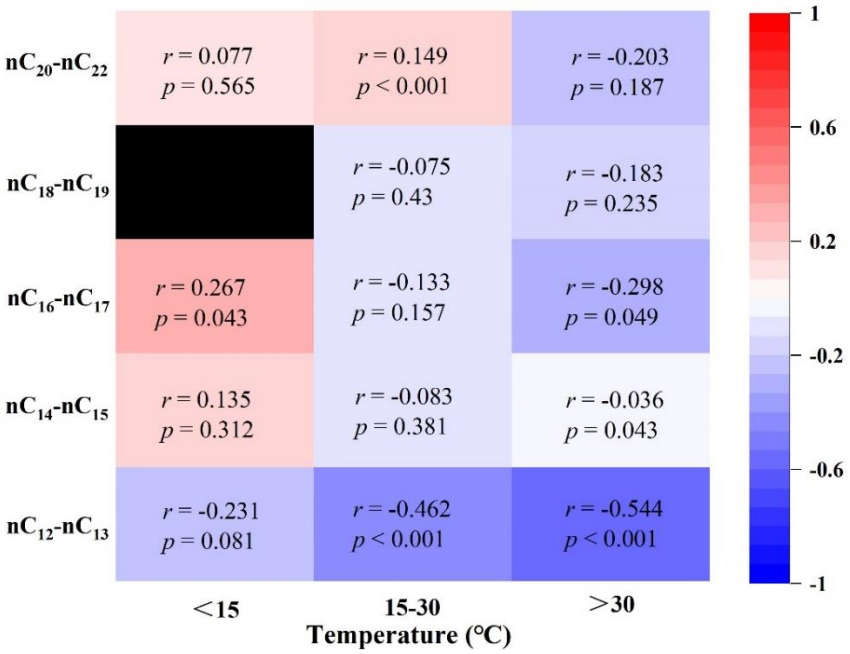


Figure S6. The correlations between IVOCs and temperature at three different temperature intervals (<15°C, 15°C−30°C, >30°C). Black denotes the missing value. When the temperature was below 15 °C, the measurement data of nC_{18}-nC_{19} species was too sparse to analyze.

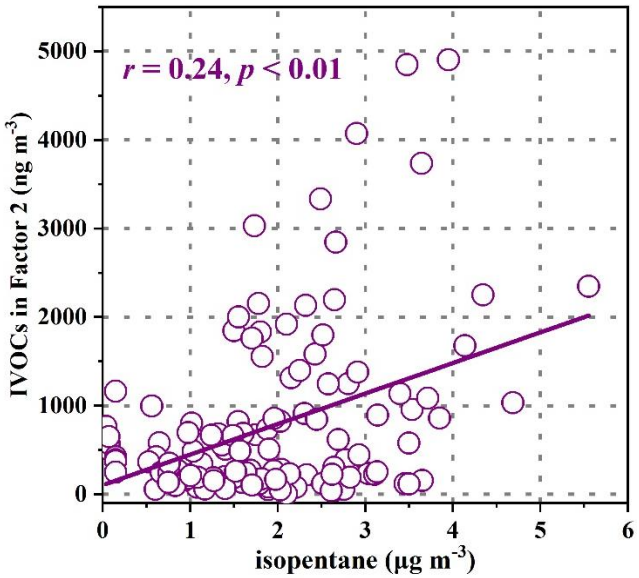


Figure S7. Correlation between IVOCs apportioned in Factor 2 and isopentane.

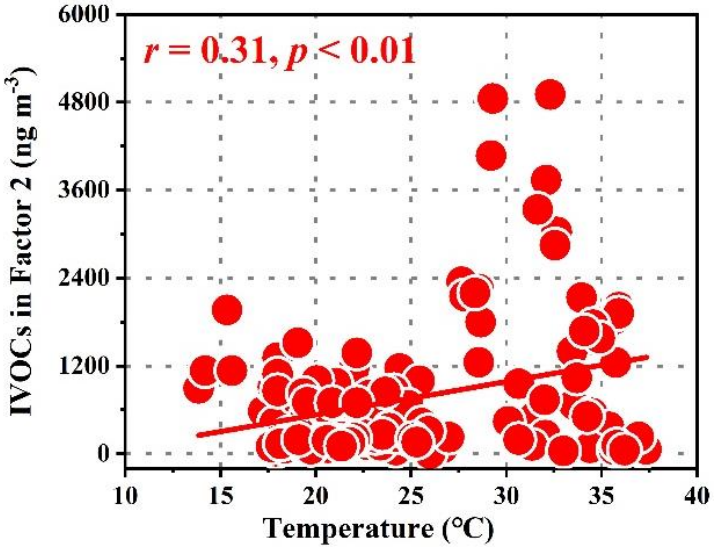


Figure S8. Correlations between IVOCs apportioned in Factor 2 and ambient temperature.

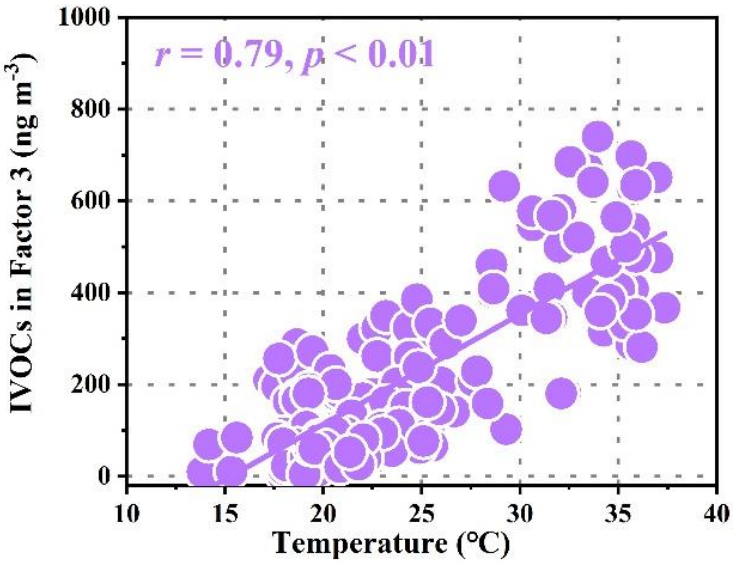


Figure S9. Correlations between IVOCs apportioned in Factor 3 and ambient temperature.

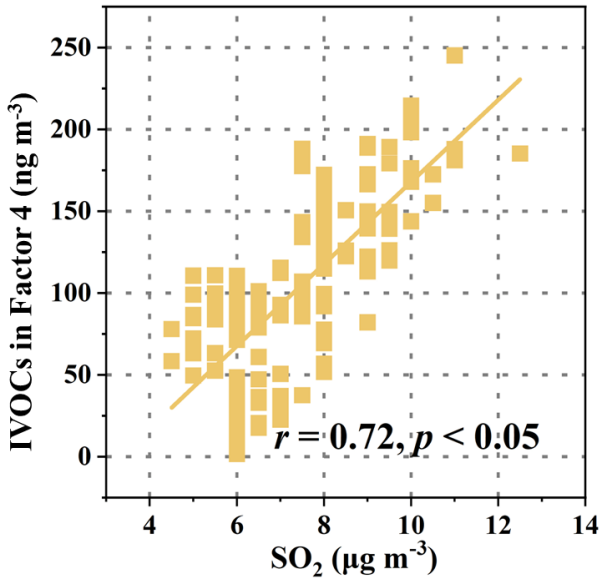


Figure S10. Correlation between IVOCs apportioned in Factor 4 and SO_2.

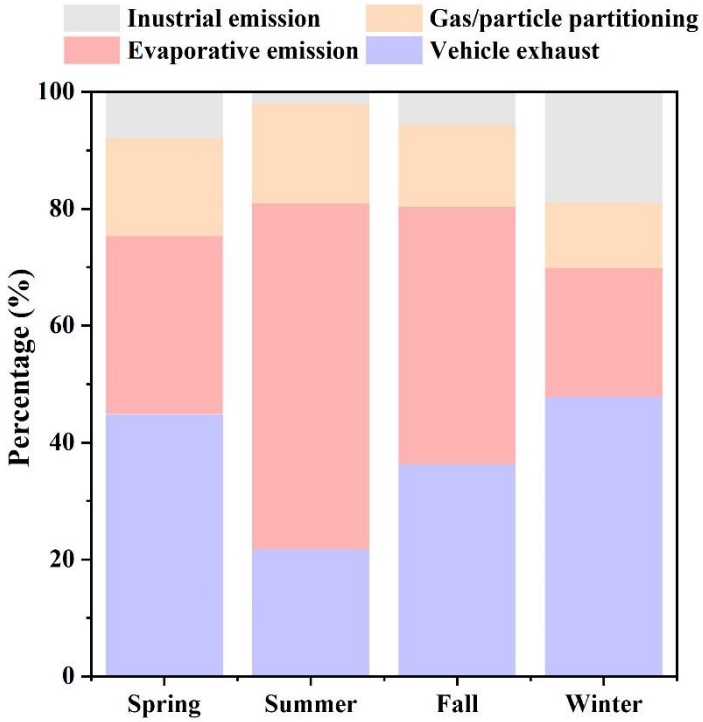


Figure S11. Relative contributions of PMF resolved sources in four seasons.

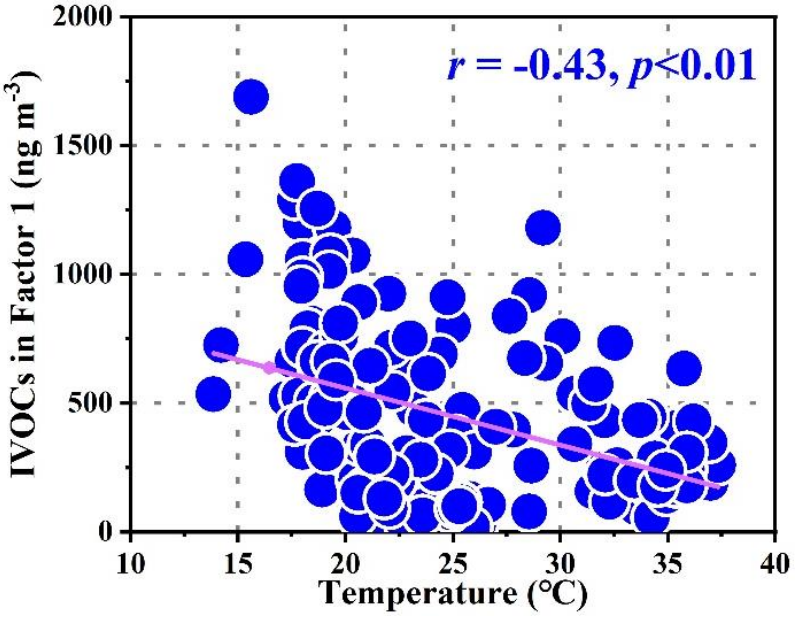


Figure S12. Correlation between IVOCs apportioned in Factor 1 and ambient temperature.

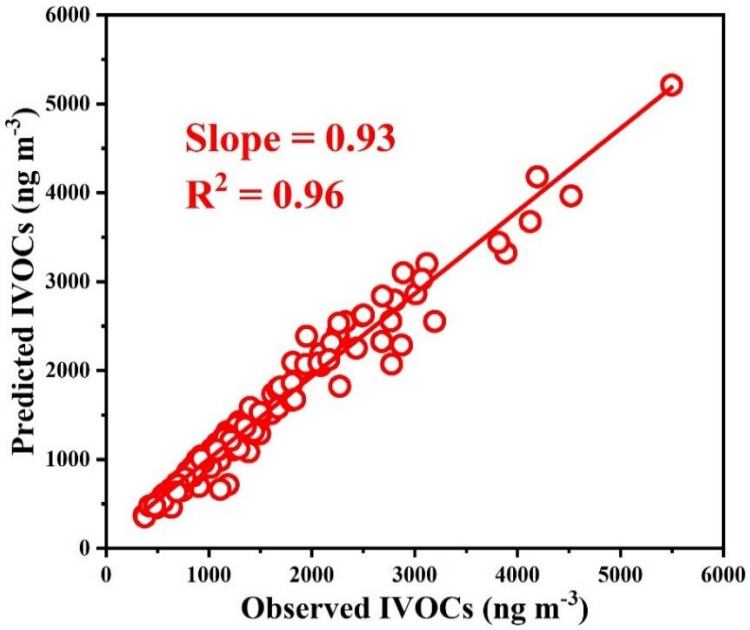


Figure S13. Comparison between observed IVOC concentrations and predictions from the PMF model.

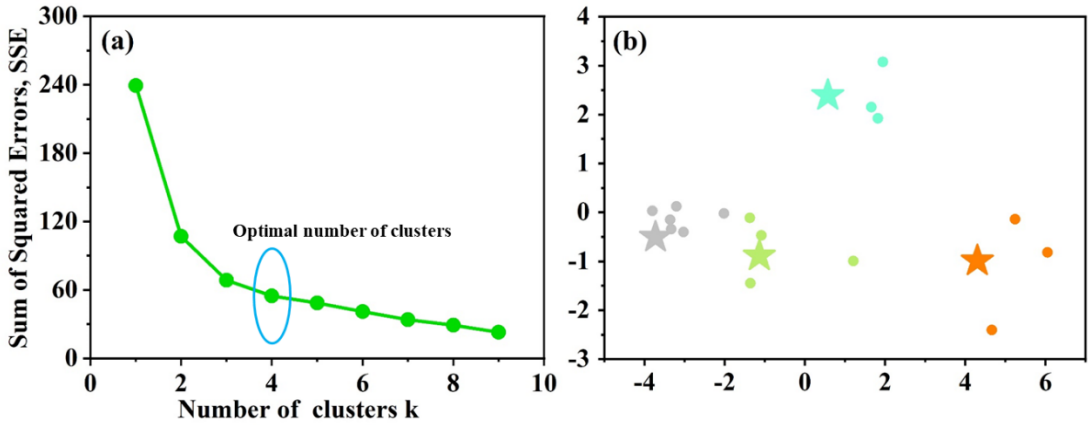


Figure S14. The optimal number of clusters based on elbow method (a) and four clustering analysis results for measured IVOCs (b). The asterisk represents cluster centroid.

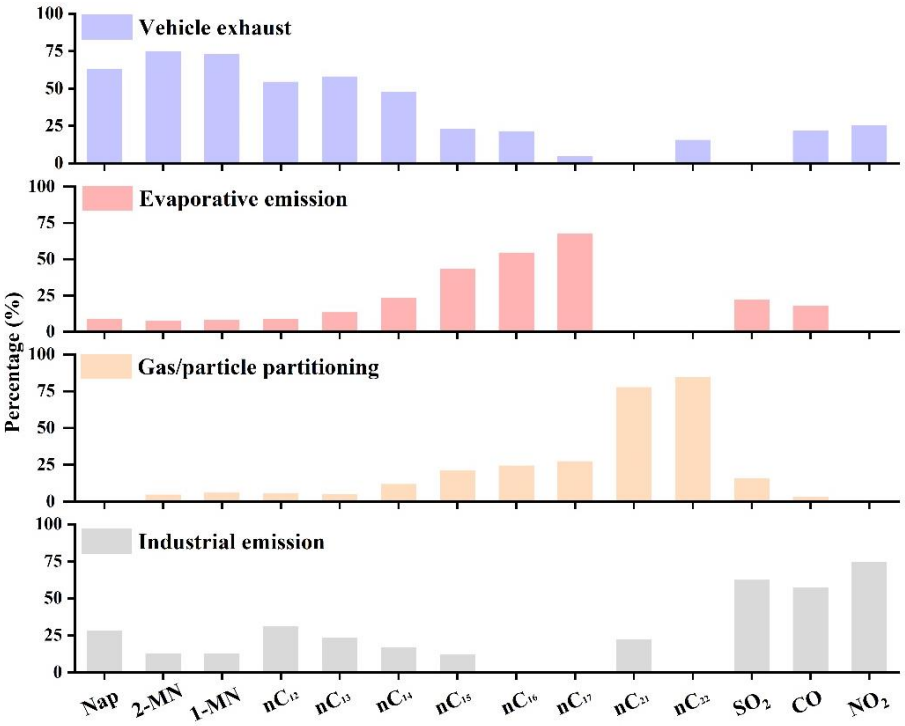


Figure S15. Factor profiles (% of the species) resolved by PMF for winter IVOC samples.

References

Fang, H., Huang, X.Q., Xiao, S.X., Lowther, S., Fu, X.W., Zhang, Y.L., Wu, T., Hu, W.W., Zhang, G.H., Ding, X., Tang, M.J., Bi, X.H., Jones, K.C., and Wang, X.M.: Intermediate-volatility organic compounds observed in a coastal megacity: Importance of non-road source emissions. J. Geophys. Res. Atmos., 127, e2022JD037301. https://doi.org/10.1029/2022JD037301, 2022.

Hartigan, J.A., and Wong, M.A.: A K-means clustering algorithm: Algorithm AS 136. Applied Statistics. 28, 100−108, https://doi.org/10.2307/2346830, 1979.

Hong, Z.; Hong, Y., Zhang, H.; Chen, J., Xu, L., Deng, J., Du, W., Zhang, Y., and Xiao, H.: Pollution characteristics and source apportionment of $PM_{2.5}$-bound n-alkanes in the Yangtze River Delta, China. Aerosol Air Qual. Res., 17, 1985−1998, https://doi.org/10.4209/aaqr.2016.12.0566, 2017.

Kang, M., Kim, K., Choi, N., Kim, Y. P., and Lee, J.Y.: Recent Occurrence of PAHs and n-Alkanes in $PM_{2.5}$ in Seoul, Korea and characteristics of their sources and toxicity. Int. J. Environ. Res. Pub. He., 17, 1397, https://doi.org/10.3390/ijerph17041397, 2020.

Lyu, Y., Xu, T.T., Yang, X., Chen, J.M., Cheng, T.T., and Li, X.: Seasonal contributions to size-resolved n-alkanes (C_8–C_{40}) in the Shanghai atmosphere from regional anthropogenic activities and terrestrial plant waxes. Sci. Total Environ., 579, 1918–1928, https://doi.org/10.1016/j.scitotenv.2016.11.201, 2016.

Tang, T.G., Cheng, Z.N., Xu, B.Q., Zhang, B.L., Li, J., Zhang, W., Wang, K.L., and Zhang, G.: Source diversity of intermediate volatility n-alkanes revealed by compound-specific $\delta^{13}C-\delta D$ isotopes. Environ. Sci. Technol., 56, 14262–14271, ttps://doi.org/10.1021/acs.est.2c02156, 2022.

Wang, J., Ho, S.S.H., Ma, S., Cao, J., Dai, W., Liu, S., Shen, Z., Huang, R., Wang, G., and Han, Y.: Characterization of $PM_{2.5}$ in Guangzhou, China: uses of organic markers for supporting source apportionment. Sci. Total Environ., 550, 961−971, https://doi.org/10.1016/j.scitotenv.2016.01.138, 2016.

Wang, Y.Q.: MeteoInfo: GIS software for meteorological data visualization and analysis. Meteorol. Appl., 21, 360-368. https://doi.org/10.1002/met.1345, 2014.

Xu, R.X., Alam, M.S., Stark, C., and Harrison, R.M.: Behaviour of traffic emitted semi-volatile and intermediate volatility organic compounds within the urban atmosphere. Sci. Total Environ., 720, 137470, https://doi.org/10.1016/j.scitotenv.2020.137470, 2020.

Yang, J., Lei, G., Liu, C., Wu, Y., Hu, K., Zhu, J., Bao, J., Lin, W., and Jin, J.: Characteristics of particulate-bound n-alkanes indicating sources of $PM_{2.5}$ in Beijing, China. Atmos. Chem. Phys., 23, 3015–3029, https://doi.org/10.5194/acp-23-3015-2023, 2023.